photonics

MDPI

Article

Comparative Study of PLSR and SVR Using MLP Feature Extraction for Quantitative Analysis of Steel Alloy Elements by Laser-Induced Breakdown Spectroscopy

Weifeng Chen and Yu Ding *

School of Mechanical and Electronic Engineering, Quanzhou University of Information Engineering, Quanzhou 362000, China
* Correspondence: yuden1989@126.com

Abstract

With the rapid development of the steel industry, the accurate detection of alloy element contents is of great significance for the evaluation of material properties and quality control. This study aims to establish a rapid, stable, and highly accurate quantitative detection method based on handheld LIBS to achieve effective analysis of key elements such as Fe, Cr, Mn, Ni, and Cu. To meet the demand of the steel industry for rapid, stable, and high-accuracy quantification of key alloy elements such as Cr, Mn, Ni, and Cu, this study was carried out on 20 types of standard steel spectral samples. Support Vector Regression (SVR) and Partial Least Squares Regression (PLSR) models were constructed, respectively. The SVR penalty factor C (0.1–10) and loss parameter ε (0.001–1), as well as the PLSR latent variable number Lv (1–20), were optimized using five-fold cross-validation repeated 100 times. Model performance was evaluated using the coefficient of determination (R^2), root-mean-square error (RMSE), and mean relative error (MRE). In the comparison of quantitative performance, excellent predictive ability for major elements such as Fe and Cr was achieved by both models; test-set R^2 values exceeded 0.92, meeting the detection requirements for high-content alloy elements. For low-content Ni, Cu, and Mn, PLSR gives R^2 values of 0.92, 0.93, and 0.89, while SVR yields 0.85, 0.49, and 0.36, showing clear limitations, especially for Cu and Mn. After introducing Multilayer Perceptron feature extraction, the R^2 of Ni, Cu, and Mn increases to 0.99, 0.99, and 0.97 for PLSR and to 0.99, 0.93, and 0.94 for SVR, with RMSE and MRE markedly reduced. In summary, the integration of LIBS with MLP feature extraction and PLSR offers both rapid processing capabilities and high precision, significantly improving the quantification of low-concentration elements, and is well-suited for real-time online monitoring in steel production, facilitating quality control and process optimization.

Keywords: steel; LIBS; quantitative analysis; MLP; SVR; PLSR

Received: 5 January 2026
Revised: 30 January 2026
Accepted: 9 February 2026
Published: 13 February 2026

1. Introduction

With the rapid development of the steel industry, the elemental composition of steel continues to diversify. The compositional differences between different steels directly determine their performance and application scenarios [1]. These differences primarily arise from the addition and regulation of alloying elements during the smelting process, where the proper ratio of alloying elements plays a crucial role in improving the overall performance of steel [2]. Chromium (Cr) is able to form a stable oxide film in steel, significantly improving corrosion resistance and heat resistance, while also enhancing hardness

and wear resistance. Therefore, it is a key element in stainless steels and heat-resistant steels [3]. Manganese (Mn) is commonly used as an important deoxidizer and desulfurizer. It improves the strength and toughness of steel, enhances hardenability, and improves hot-working performance. However, excessive Mn can increase the brittleness of steel [4]. Nickel (Ni) is renowned for improving toughness, strength, and corrosion resistance, particularly in maintaining mechanical properties at low temperatures [5]. Copper (Cu) forms a stable protective oxide film in steel, significantly improving atmospheric corrosion resistance. It also enhances strength and wear resistance through solid solution and precipitation strengthening. However, excessive Cu can lead to thermal brittleness [6]. Thus, controlling the content of Cr, Mn, Ni, and Cu is crucial for ensuring steel quality [7]. Therefore, there is an urgent need to establish a high-precision, rapid, and real-time applicable analysis method to achieve accurate detection and strict control of these key elements. This also imposes higher technical requirements for detecting the elements and their concentrations in raw materials, thereby contributing to the improvement of the accuracy and reliability of detection results.

Laser-Induced Breakdown Spectroscopy (LIBS) is a spectral analysis technique with great potential for online, in situ, rapid, and multiple-element detection [8–11]. It plays a significant role in the real-time analysis of key elements in steel. Zheng et al. [12] and Chen et al. [13] have been committed to improving the precision and stability of LIBS in steel analysis. By combining LIBS with plasma imaging screening methods, the detection performance of Cu, Cr, and Mn in steel was significantly improved. Compared with the raw spectra, R_P^2 (coefficient of determination of prediction) increased from 93% to nearly 99%, and the values of $RMSE_P$ (root-mean-square error of prediction) and MRE_P (mean relative error of prediction) were reduced by more than 50%. Zhang et al. [14] and Yang et al. [15] improved LIBS data-processing methods by enhancing chemometric preprocessing to improve the accuracy of qualitative and quantitative analysis, and by proposing an improved piecewise Hermite cubic interpolation method and a wavelet-transform-based empirical mode decomposition (EMD) method, which effectively reduced spectral noise and improved detection accuracy; in particular, the mean relative error for Cr decreased from 10% to 3.8%. Traparić et al. [16] and Yang et al. [17] also made important contributions. The former compared the performance of three models—random forest (RF), L2 linear regression, and deep neural networks (DNN)—in predicting the composition of austenitic steel samples. The results showed that RF provided the best prediction performance, while DNN outperformed linear regression [18]. The latter applied transfer learning by transferring room-temperature spectral data to high-temperature conditions to improve alloy steel analysis, and the mean absolute error and relative error of the test samples were reduced by 13% and 20%, respectively. Brunnbauer et al. [19] and Li et al. [20] highlighted methodological challenges in LIBS applications, noting that classification algorithms in LIBS are often treated as "black boxes." Inadequate or improper handling of essential procedures may lead to overestimated performance and unreliable assessment of generalization. They also pointed out issues such as overfitting and limited interpretability, emphasizing the need to improve model transparency and adopt more robust approaches.

The diversification of elemental composition in steel, especially the inclusion of low-concentration elements such as Mn, Ni, and Cu, poses a major challenge for online quantitative analysis. The low proportions of these elements lead to weak spectral signals that are easily masked by noise, interference, and matrix effects, so conventional full-spectrum or line-selection strategies struggle to maintain high precision. Meanwhile, due to limitations in computational efficiency and real-time applicability, existing studies still fall short of meeting the practical requirements of production-line online monitoring. To address

this, this study develops SVR and PLSR models from LIBS spectra of 20 standard steel samples, using handheld LIBS devices for data collection, and introduces a nonlinear feature-extraction method to reduce data dimensionality. By extracting key features and reducing data dimensionality, the models' predictive power was increased.

2. Materials and Methods

2.1. Experimental Setup

The data were collected using a handheld Laser Induced Breakdown Spectrometer (LMHJ.B02, Aliben Ltd., Chengdu, China). The spectrometer operates with a laser source that emits at a wavelength of 1535 nm, with a pulse energy of approximately 40 μJ and a pulse width of 5 ns. The laser frequency is set to 1000 Hz, providing rapid and efficient measurements. The instrument has a detection range of 180 nm to 440 nm for a single channel, ensuring comprehensive spectral analysis for a variety of alloy elements. During measurements, the detector integration time was set to 50 ms, and the gate delay was set to 100 ns to optimize signal acquisition.

2.2. Experimental Samples and Data Acquisition

The samples used in this study are spectral standards, with a total of 20 samples. Each sample was processed into a cylindrical shape with a diameter of φ45 mm and a thickness of 35 mm. To avoid the influence of non-representative surface compositions and surface texture on the plasma, the sample surfaces were polished with sandpaper before measurements. The main elements in these samples included Fe, Mn, Cr, Ni, Cu, and others, with specific contents shown in Table 1. During the experiment, 100 measurement points were randomly selected for each sample, and a single spectral acquisition was performed at each point, resulting in a total of 2000 spectral data points. To reduce the impact of random noise, the 100 spectra for each sample were averaged to obtain one representative spectrum, ultimately forming 20 sets of representative spectral data for each standard sample. Subsequently, these 20 sets of data were divided into a training set and a test set in a 7:3 ratio, with 14 sets used for training and 6 sets used for testing.

Table 1. Designations and elemental compositions (wt%) of 20 steel samples.

Label	Grade	Fe	Cr	Cu	Ni	Mn	Label	Grade	Fe	Cr	Cu	Ni	Mn
1#	YSBS453251-2019	90.54	2.5	0.024	2.42	0.082	11#	YSBS 11231-2013	95.67	2.94	0.057	0.03	0.576
2#	YSBS454120-2014	91.03	4.96	0.044	0.05	0.34	12# *	YSBS41307a-2011	70.22	17.3	0.316	9.25	1.47
3# *	YSBS41108-2010	95.6	0.04	0.109	0.05	0.573	13#	OPTS351058-2020	96.85	1.46	0.055	0.01	0.352
4#	YSBS41109-2010	98.01	0.19	0.185	0.23	0.533	14#	JZK223	95.57	1.5	0.05	0.11	1.15
5#	YSBS31405-2015	95.62	1.05	0.062	0.15	0.873	15# *	YSBS20120C-2009	81.18	4.02	0.075	0.06	0.318
6# *	YSBS41324-2010	97.40	1.02	0.062	0.02	0.611	16#	9Cr2MoV	95.72	1.94	0.2	0.09	0.39
7#	YSBS201200-2009	84.83	11.6	0.082	0.1	0.155	17#	K192A	83.19	12.1	0.30	0.32	0.25
8#	YSBS41406-2013	90.62	5.06	0.079	0.19	0.34	18# *	OPTS351075-2021	92.32	1.3	0.018	3.25	0.385
9# *	YSBS 11475-2001	95.02	1.13	0.131	0.09	0.935	19#	TSK109a	88.09	8.06	0.293	0.74	0.408
10#	YSBS18111-2005	98.47	-	-	-	0.553	20#	K199	91.81	4.75	0.19	0.65	0.38

* represents test set data.

2.3. Experimental Method

In this study, Laser-Induced Breakdown Spectroscopy (LIBS) was utilized for the quantitative analysis of key alloy elements such as Fe, Cr, Mn, Ni, and Cu in steel samples. The process began with spectral acquisition, where raw spectral data were collected using the LIBS technique. The acquired spectra were then subjected to data preprocessing, which included baseline correction to ensure the accuracy and reliability of the data. Following preprocessing, model training was performed using Support Vector Regression (SVR) and Partial Least Squares Regression (PLSR) models. The hyperparameters of the models, including the SVR penalty factor C, loss parameter ε, and the number of latent variables (Lv) for PLSR, were optimized through a five-fold cross-validation repeated 100 times to

achieve optimal model performance. By introducing Multilayer Perceptron feature extraction, the original 2048-dimensional spectral features were compressed into 128-dimensional representations. This dimensionality reduction was carried out to eliminate redundant features and improve computational efficiency. Finally, the trained models were used for prediction, and the model prediction results were output to provide precise quantification of the alloy element concentrations in the steel samples. This process facilitated both the optimization of model performance and the enhancement of prediction accuracy, particularly for low-concentration elements. The overall workflow of the experiment is shown in Figure 1, which outlines the sequence from spectral acquisition to model prediction output.

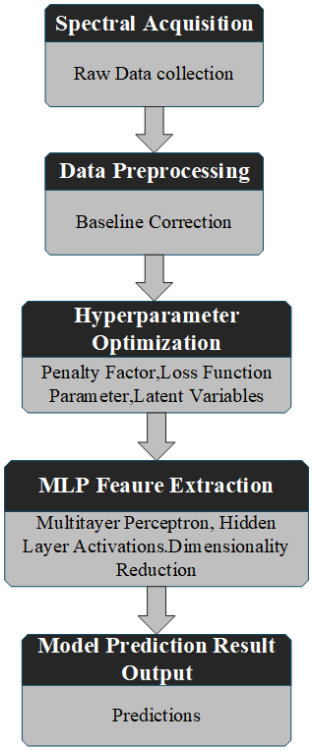

Figure 1. Workflow of experimental methodology.

To further improve the quantitative performance of sample concentration prediction, this study employs a MLP for feature extraction from spectral data. The method uses a multi-layer fully connected structure to perform layer-by-layer nonlinear mapping of the input spectra, progressively extracting deep features related to changes in sample concentration.

The MLP network consists of three fully connected layers, with each layer performing dimensionality reduction and reorganization of spectral features to enhance their expressive power. After each fully connected layer, batch normalization, LeakyReLU activation functions, and dropout regularization are introduced to stabilize the training process. The structure design enables the MLP to automatically learn key features from the spectral data that are strongly correlated with sample concentration. During the training process, the spectral dataset is randomly divided into a training set and a test set with a 7:3 ratio.

In this study, two machine learning algorithms were employed: Support Vector Regression (SVR) and Partial Least Squares Regression (PLSR). Model performance was comprehensively evaluated using R^2, RMSE, and MRE [21–23]. The coefficient of determination (R^2) is a statistical measure that indicates the fit of a regression model to the data. It represents the proportion of the variance in the dependent variable that is explained by the independent variables in the model.

(1) Support Vector Regression (SVR) was proposed by Vapnik et al. on the basis of Support Vector Machine (SVM) theory and has been widely applied to nonlinear regression and spectral quantitative analysis [24]. Its core idea is that a regression function is constructed in a high-dimensional feature space while the model complexity is minimized and the deviation between predicted and true values is constrained within a given threshold ε as much as possible [25]. The factor C controls the trade-off between error tolerance and model complexity, and parameter ε determines the sensitivity of the model to small errors.

(2) Partial Least Squares Regression (PLSR) is a multivariate statistical method commonly used for the analysis of high-dimensional and multicollinear data. Its core idea is to extract latent variables (Lv) in order to maximize the correlation between independent and dependent variables while reducing dimensionality, thereby achieving stable modeling performance [26]. Since LIBS spectra are characterized by high dimensionality and severe feature overlap, the PLSR model can balance data compression and modeling accuracy when dealing with such data, and thus it has been widely applied to the quantitative analysis of material composition [27].

3. Results and Discussion

3.1. Qualitative Analysis

The baseline-corrected average spectrum using Adaptive Iteratively Reweighted Penalized Least Squares (AIRPLS) of the 12# steel sample YSBS41307a-2011 is shown in Figure 2. From the overall spectral distribution and comparison with the NIST database [28], numerous strong characteristic lines are observed in the 200 nm–450 nm range, with the 230 nm–290 nm region being the most concentrated. These characteristic lines primarily correspond to Fe, reflecting the characteristic features of iron as the matrix element of steel. Characteristic lines of several alloying elements are also observed, including Cr at 283.56 nm, 425.53 nm, 427.48 nm, and 428.93 nm; Ni at 221.64 nm, 300.24 nm, 357.87 nm, and 359.35 nm; Mn at 260.57 nm and 403.07 nm; and Cu at 324.75 nm. These characteristic lines provide crucial spectral evidence for subsequent quantitative analysis and modeling.

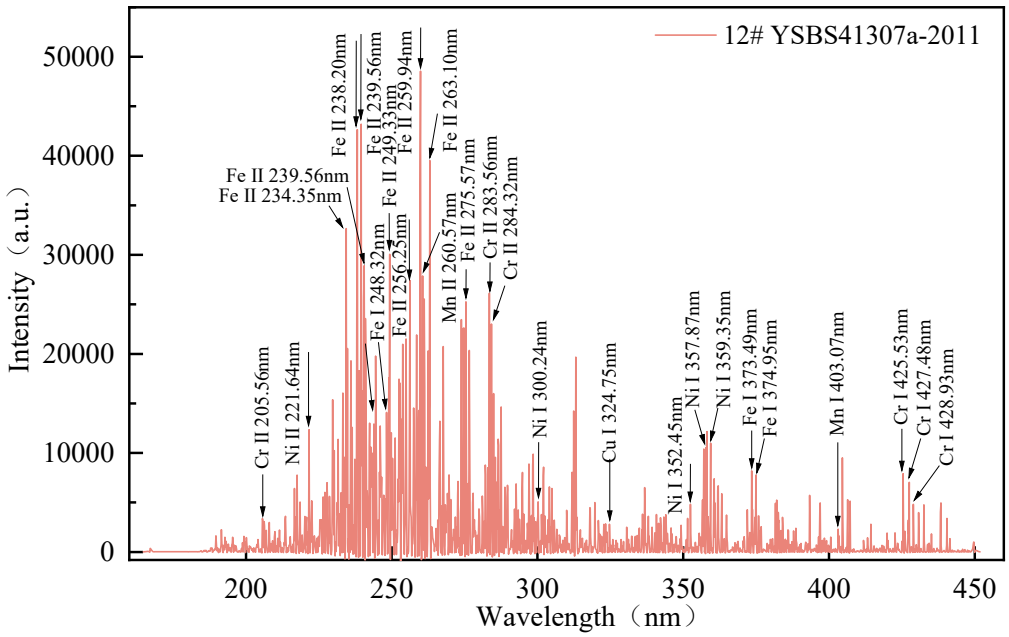

Figure 2. LIBS spectrum of the 12# steel sample.

3.2. Quantitative Analysis

3.2.1. Quantitative Analysis of the SVR Model

In terms of parameter optimization, the two key hyperparameters—the penalty factor C and the loss function parameter ε—were tuned by combining grid search with five-fold cross-validation repeated 100 times, with C = {0.1, 0.3, 1, 3, 10} and ε = {0.001, 0.003, 0.01, 0.03, 0.1, 0.3, 1}. Cross-validation was conducted only within the training set, and the test set was used solely for the final evaluation.

SVR cross-validation results for Fe, Cr, Ni, Cu, and Mn under varying penalty factors C and loss parameters ε are shown in Figures 3–7. Overall, model performance for each element was sensitive to the hyperparameter settings, and a consistent trend was observed. Within the small-ε range (0.001–0.03), low $RMSE_{CV}$ (root-mean-square error of cross-validation) and high R^2_{CV} (coefficient of determination of cross-validation) were maintained. When $\varepsilon \geq 0.1$, $RMSE_{CV}$ generally increased, and R^2_{CV} decreased markedly. This indicates that an excessively large ε reduces the model's ability to discriminate differences in the data. The penalty factor C also affected prediction: overly small values of C (0.1 or 0.3) resulted in underfitting; when C = 10, prediction accuracy and stability were improved significantly.

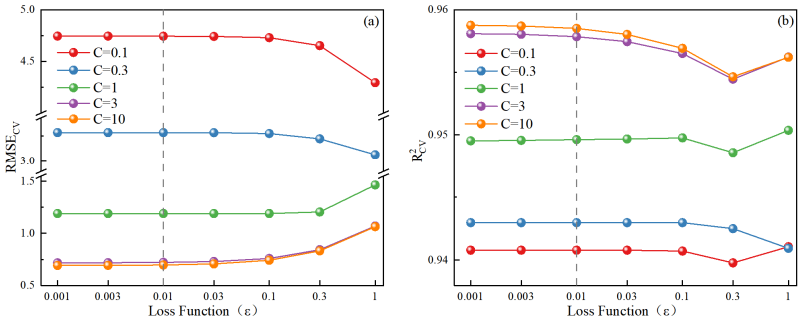

Figure 3. Parameter optimization of the SVR model for Fe element ((**a**): $RMSE_{CV}$, (**b**): R^2_C).

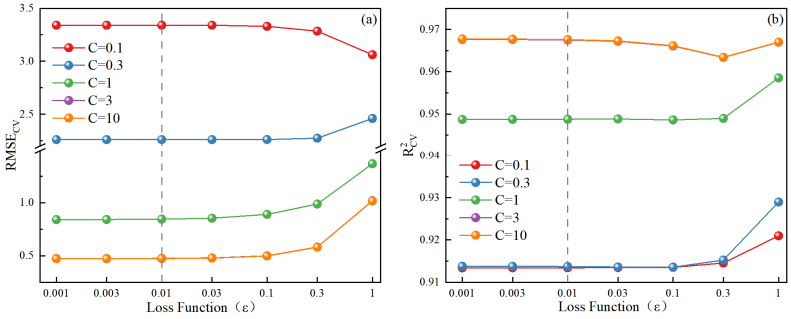

Figure 4. Parameter optimization of the SVR model for Cr element ((**a**): $RMSE_{CV}$, (**b**): R^2_{CV}).

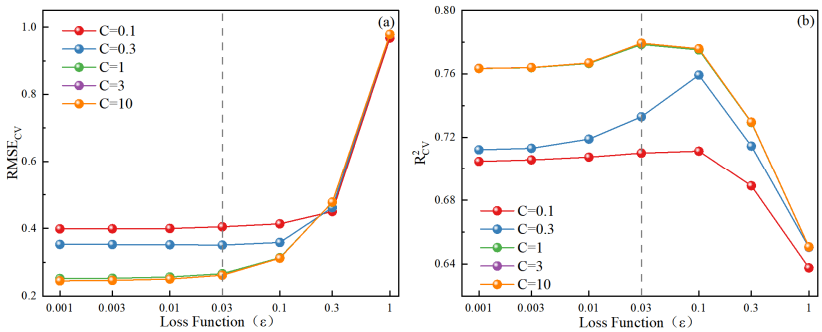

Figure 5. Parameter optimization of the SVR model for Ni element ((**a**): $RMSE_{CV}$, (**b**): R^2_{CV}).

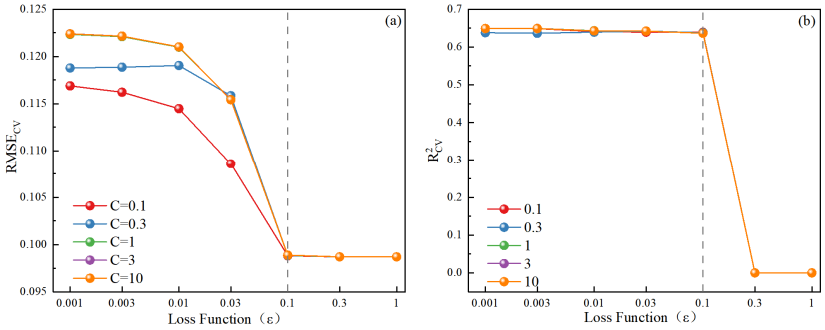

Figure 6. Parameter optimization of the SVR model for Cu element ((**a**): $RMSE_{CV}$, (**b**): R^2_{CV}).

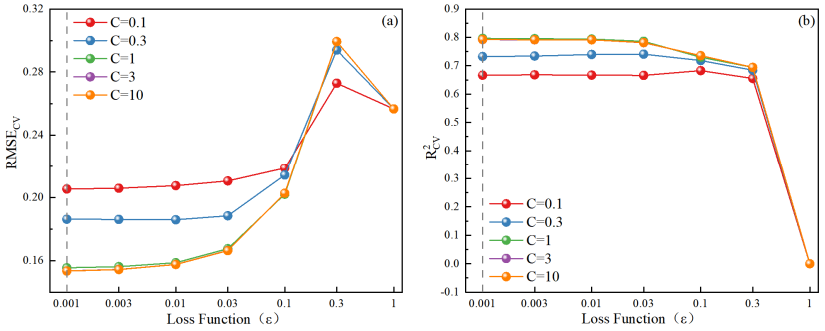

Figure 7. Parameter optimization of the SVR model for Mn element ((**a**): $RMSE_{CV}$, (**b**): R^2_{CV}).

From the element-specific analyses, optimal performance for Fe and Cr was obtained at C = 10 and ε = 0.01–0.03. $RMSE_{CV}$ decreased to approximately 0.75 and 0.50, and the corresponding R^2_{CV} values exceeded 0.95, indicating high quantitative predictive accuracy. For Ni, the optimum occurred at ε = 0.03 (R^2_{CV} = 0.78), with a rapid decline for ε ≥ 0.1. For Cu, the overall error was low ($RMSE_{CV}$ = 0.11). Within the small ε range, R^2_{CV} was maintained near 0.70, but a sharp deterioration was observed when ε < 0.1. For Mn, stable behavior was observed at ε ≤ 0.03 ($RMSE_{CV}$ = 0.16–0.20; R^2_{CV} maintained at 0.75–0.85), whereas performance decline occurred when ε ≥ 0.3.

Combinations of C and ε were cross-validated to optimize predictive performance, and optimal parameters were determined from $RMSE_{CV}$ and R^2_{CV} trends. Specifically, the optimal parameters of the SVR model are C = 10, ε = 0.01 for Fe; C = 3, ε = 0.01 for Cr; C = 3, ε = 0.03 for Ni; C = 0.1, ε = 0.1 for Cu; and C = 3, ε = 0.001 for Mn. On this basis, further prediction analysis was carried out on the test set to evaluate the practical application value of the model under the selected parameters.

After the optimal parameter combinations were determined, the SVR models for each element were applied to the test set for validation, and the results are shown in Figure 8. Overall, the predicted values and the true values of the five elements exhibited varying degrees of linear correlation. However, the fitting accuracy differed markedly due to variations in elemental concentrations and spectral characteristics.

As shown in Figure 8, panels (a–e) plot the linear fits between measured and predicted concentrations for five elements in steel (Fe, Cr, Ni, Cu, Mn). For Fe, a correlation of R^2_P = 0.92 was obtained, with $RMSE_P$ = 2.69 and MRE_P = 0.03. These results indicate that the SVR model shows good predictive performance for this element, characterized by a high correlation with the true values and small prediction errors. The Fe concentration can be predicted with reasonable accuracy. For Cr, R^2_P reached 0.98, with $RMSE_P$ = 0.90 and MRE_P = 1.80. These results indicate a high agreement between predicted and true values, low prediction error, and good stability. The model can predict the Cr concentration accurately. For Ni, R^2_P = 0.85 was obtained, with $RMSE_P$ = 1.31 and MRE_P = 1.91. This

indicates that the SVR model predicts Ni less accurately than Fe and Cr, the association with the true values was reduced, and the errors were larger.

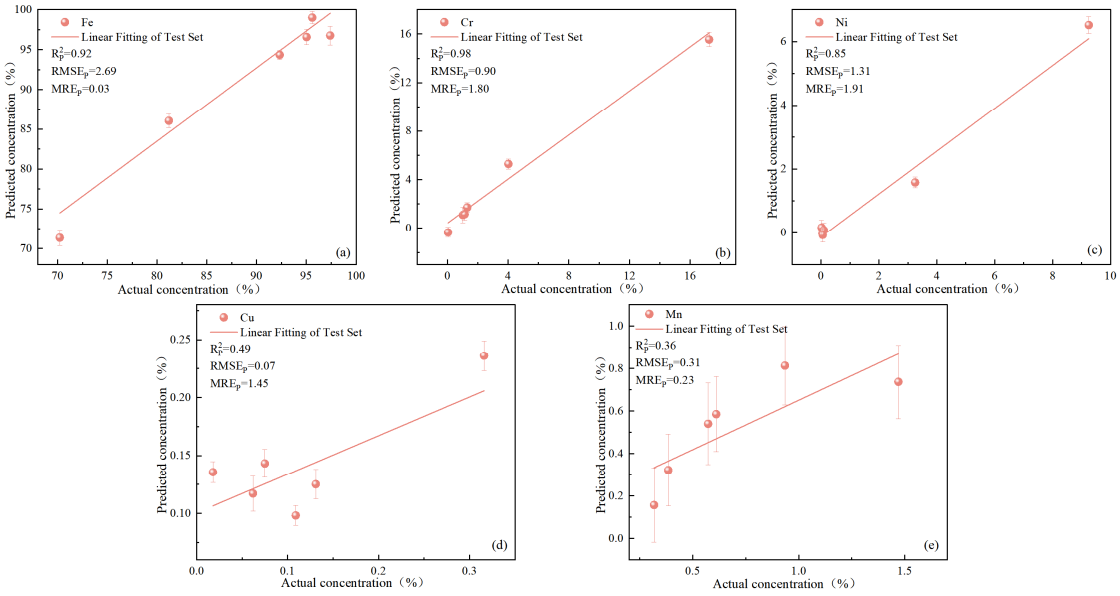

Figure 8. Test set prediction of different elements using the SVR model ((**a**): Fe, (**b**): Cr, (**c**): Ni, (**d**): Cu, (**e**): Mn).

In contrast, R_P^2 = 0.49, $RMSE_P$ = 0.07, and MRE_P = 1.45 were obtained for Cu, while R_P^2 = 0.36, $RMSE_P$ = 0.31, and MRE_P = 0.23 were obtained for Mn. The data points for both Cu and Mn were scattered, and deviations between predicted and measured values were evident, indicating low linear correlation with the measured values and limited prediction performance. As a result, the overall predictive effect for these trace elements is inadequate.

As shown in Figure 9, Fe exhibits relatively low and stable RSD_P (relative standard deviation of prediction) values, indicating stable spectral responses and good predictive performance. The RSD_P values for Cr and Ni also demonstrate stability prediction results, indicating that predictions for these elements are reliable. However, for trace elements like Cu and Mn, higher RSD_P values are observed, reflecting lower stability in the predictions for trace elements.

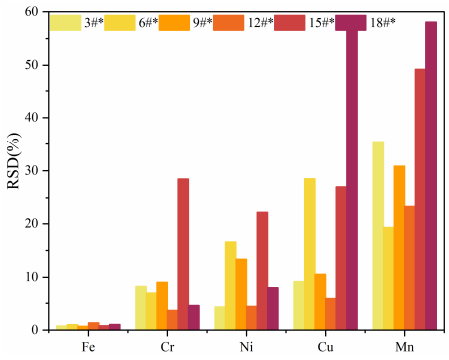

Figure 9. RSD of prediction for different elements using the SVR model.

3.2.2. Quantitative Analysis of the PLSR Model

To obtain optimal model performance, a five-fold cross-validation repeated 100 times was conducted within the training set to search and compare the number of latent variables Lv in the range of 1–20, with the corresponding $RMSE_{CV}$ and R_{CV}^2 of cross-validation recorded. Cross-validation was conducted only within the training set, and the test set was used solely for the final evaluation.

Figure 10 shows the PLSR cross-validation results for Fe, Cr, Ni, Cu, and Mn at different Lv. As the number of latent variables increased, R^2_{CV} and $RMSE_{CV}$ varied in a regular manner. $RMSE_{CV}$ was higher at small Lv, then decreased and tended to stabilize as Lv increased. Correspondingly, R^2_{CV} rose initially with Lv and then remained stable within a certain range.

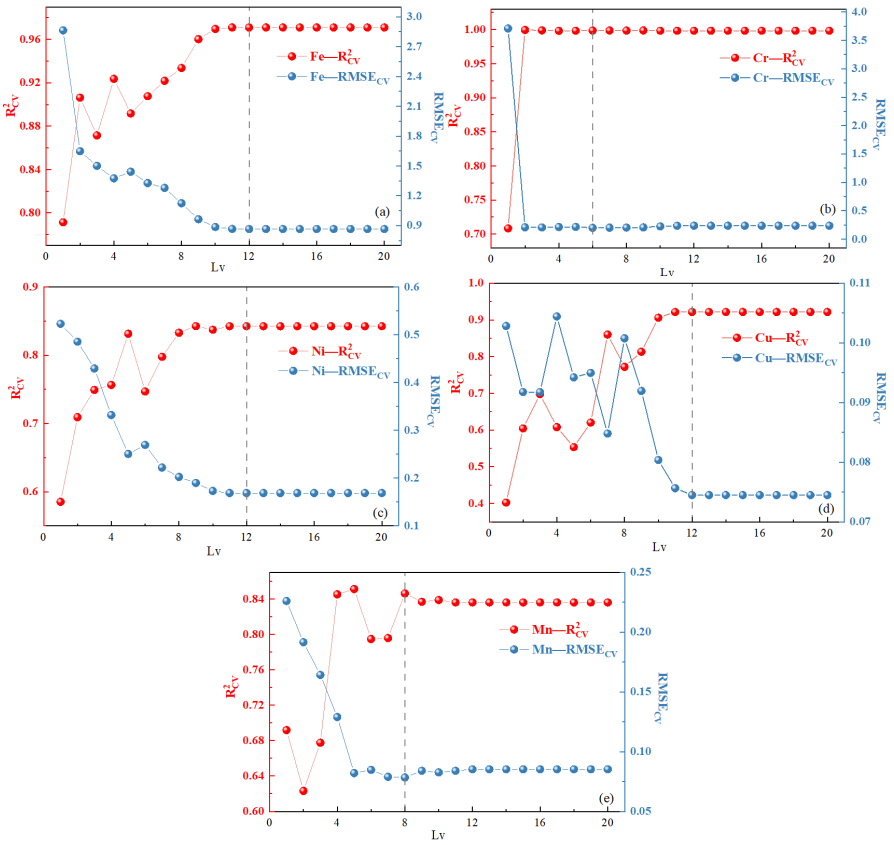

Figure 10. Parameter optimization of the PLSR model for different elements ((**a**): Fe, (**b**): Cr, (**c**): Ni, (**d**): Cu, (**e**): Mn).

For Fe, the best performance was obtained at Lv = 12, with R^2_{CV} maintained above 0.97 and $RMSE_{CV}$ reduced to about 0.9, indicating strong fitting ability. For Cr, performance was particularly strong, with optimal results at Lv = 6, where R^2_{CV} = 0.99 and $RMSE_{CV}$ approached 0, suggesting a strong linear relationship between spectral features and concentration. For Ni, the optimum occurred at Lv = 12 (R^2_{CV} = 0.85, $RMSE_{CV}$ = 0.3), indicating slightly lower predictive performance than for the main elements but acceptable applicability. For Cu, optimal performance was achieved at Lv = 12, with R^2_{CV} = 0.93 and $RMSE_{CV}$ stabilized at 0.07–0.08, indicating promising predictive potential. For Mn, the optimal Lv was eight, with R^2_{CV} = 0.84 and $RMSE_{CV}$ = 0.1, and the overall performance exceeded that of the SVR model, indicating an advantage of PLSR for Mn.

The PLSR model exhibits high accuracy and stability in the quantitative modeling of major alloy elements such as Fe and Cr, and also shows certain applicability for low-content elements such as Ni, Cu, and Mn, with the fitting results for Cu and Mn significantly better than those of the SVR model. This indicates that PLSR can effectively utilize latent variables to extract spectral information and has promising predictive performance in the analysis of complex spectral data.

After determining the optimal number of latent variables, the PLSR model was applied to the test set for validation, and the results are presented in Figure 11. As shown in panels (a–e), linear fits between measured and predicted concentrations for Fe, Cr, Ni, Cu, and

Mn in steel are presented under the PLSR model. For Fe, R_P^2 = 0.92, $RMSE_P$ = 2.77, and MRE_P = 0.02 were obtained, indicating a high correlation with the reference values and a generally low error level. For Cr, R_P^2 reached 0.98, with $RMSE_P$ = 0.75 and MRE_P = 0.70. The data points are closely clustered, indicating strong agreement between predicted and measured values, low error, and precise concentration estimation. For Ni, with R_P^2 = 0.92, $RMSE_P$ = 0.98, and MRE_P = 0.76, high correlation with the measured values was observed; the points were closely aligned with the fitted line, indicating reliable and stable predictions. For Cu, R_P^2 = 0.93, $RMSE_P$ = 0.02, and MRE_P = 0.47 were achieved. Close agreement with the measurements and small errors were observed. Overall, effective quantification of Cu is supported. For Mn, R_P^2 = 0.89, $RMSE_P$ = 0.13, and MRE_P = 0.20 were obtained. Although deviations were observed at the lowest and highest test concentrations, the overall deviations remained small, indicating that the Mn concentration can be predicted effectively.

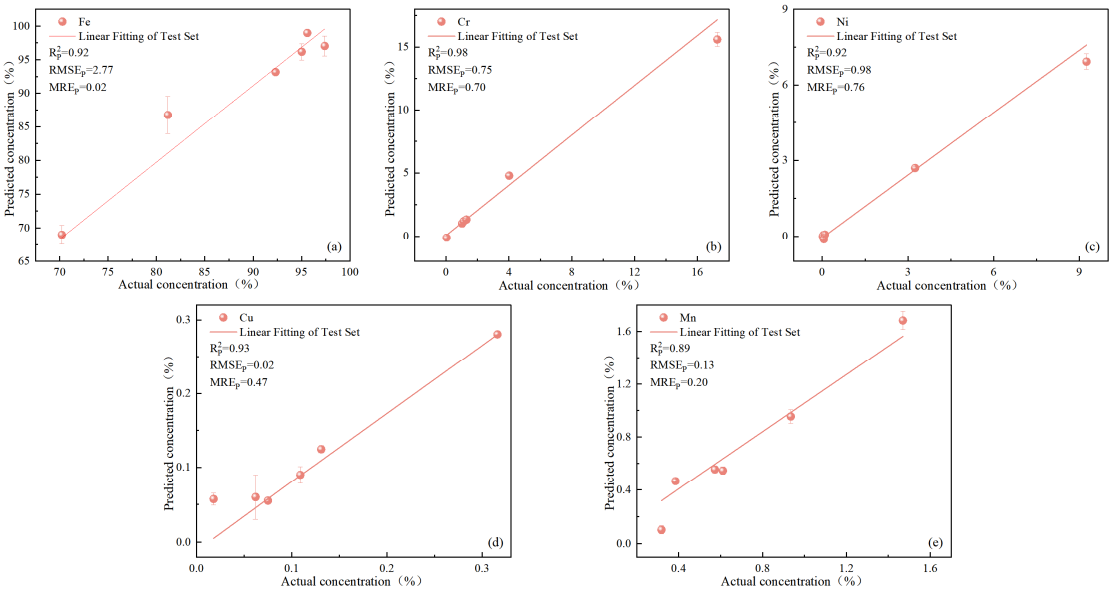

Figure 11. Test set prediction plots of different elements using the PLSR model ((**a**): Fe, (**b**): Cr, (**c**): Ni, (**d**): Cu, (**e**): Mn).

As shown in Figure 12, Fe shows low and stable RSD_P, indicating good predictive performance. The RSD_P values for Cr and Ni are also low, indicating high stability in the predictions. Even for trace elements like Cu and Mn, the RSD_P for the predicted values remains within an acceptable range, suggesting that the model can still provide reasonably accurate predictions for low-concentration elements.

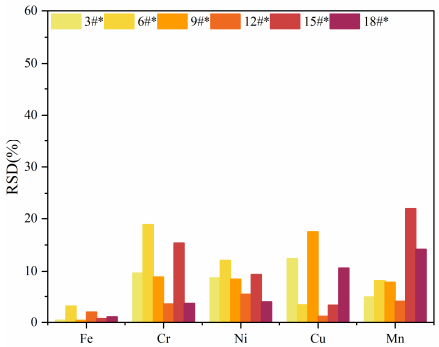

Figure 12. RSD of predictions for different elements using the PLSR model.

3.2.3. Comparison of Model Predictive Performance

As shown in Table 2, the PLSR model was found to outperform the SVR model overall on the test sets of Fe, Cr, Ni, Cu, and Mn. In the predictions for Fe and Cr, high R_P^2, low $RMSE_P$, and MRE_P, and short error bars were observed for both models, whereas for Ni, a gain with PLSR over SVR was observed with R_P^2 higher by 0.07 and $RMSE_P$ and MRE_P lower by 0.33 and 1.15, respectively. The most pronounced differences were seen for Cu and Mn. For Cu, a substantial improvement with PLSR was observed, with R_P^2 increasing from 0.49 under SVR to 0.93, and the error bars becoming markedly shorter than under SVR, indicating enhanced prediction stability. For Mn, superior performance with PLSR was also observed, with R_P^2, $RMSE_P$, and MRE_P improved over SVR by 0.53, 0.18, and 0.03; the error bars were noticeably decreased, indicating concurrent gains in stability and prediction accuracy. The differences in performance can be attributed to the nature of the models: SVR is a nonlinear model, whereas PLSR is linear. As a result, PLSR is better suited for cases where the relationship between spectral features and element concentration is approximately linear. Additionally, PLSR assigns weights to variables based on their variance and correlation, which helps it handle complex spectral data more effectively, especially when there is spectral overlap or multicollinearity among variables.

Table 2. Comparison of classification results of the two models.

Model	Element	R_P^2	$RMSE_P$	MRE_P
PLSR	Fe	0.92	0.0277	0.0002
	Cr	0.98	0.0075	0.0070
	Ni	0.92	0.0098	0.0076
	Cu	0.93	0.0002	0.0047
	Mn	0.89	0.0013	0.0020
SVR	Fe	0.92	0.0269	0.0003
	Cr	0.98	0.0090	0.0180
	Ni	0.85	0.0131	0.0191
	Cu	0.49	0.0007	0.0145
	Mn	0.36	0.0031	0.0023

In summary, PLSR outperformed SVR on the key indices (R^2, $RMSE_P$, MRE_P) across the five elements: for Fe and Cr, performance was comparable to the SVR model at a similarly high level, whereas for Ni, Cu, and Mn, superior results over SVR were observed, indicating stronger overall predictive capability.

3.2.4. MLP Feature Extraction

To further enhance the model's predictive capability, a feature extraction step was introduced before the PLSR and SVR models, using a Multi-Layer Perceptron (MLP) for feature extraction [29]. The output layer of the MLP was set to 128 dimensions, reducing the original 2048-dimensional feature data to 128 dimensions, resulting in decreased data dimensionality and improved computational efficiency. This approach can effectively capture key information from the spectral data while eliminating redundant features, providing more concise input for the subsequent PLSR and SVR models. Before feature extraction, the runtime for PLSR was 1.17 s, whereas after extraction, it was reduced to 0.15 s. For SVR, the runtime before feature extraction was 1.92 s, and it was reduced to 0.15 s after extraction. The optimized PLSR and SVR models were validated on the test set and compared with the results of the original data without feature extraction. The results showed that after feature extraction, the predictive performance of both the PLSR and SVR models improved, especially for low-concentration elements such as Ni, Cu, and Mn, with R^2 values and other evaluation metrics showing improvements.

As shown in Table 3, after MLP feature extraction, the performance of both the PLSR and SVR models significantly improved across all elements. The R^2 values for all elements (Fe, Cr, Ni, Cu, and Mn) increased, with Fe, Cr, Ni, and Cu reaching R^2 values of 0.99. Specifically, the PLSR model demonstrated strong predictive performance for Fe (0.98), Cr (0.99), Ni (0.99), Cu (0.99), and Mn (0.97), with very low $RMSE_P$ and MRE_P values, particularly for Ni and Cu, indicating that feature extraction significantly improved model accuracy and reduced prediction errors. The SVR model also showed improvement, with R^2 values for Fe (0.99), Cr (0.99), Ni (0.99), and Cu (0.93). However, for Cu, SVR performed slightly worse than PLSR, with R^2 of 0.93 and $RMSE_P$ of 0.0007, though still demonstrating effective prediction capabilities. Notably, after MLP feature extraction, the prediction accuracy for Cu and Mn significantly improved, with Cu achieving R^2 values of 0.99 in both PLSR and SVR models, compared to 0.93 in SVR without feature extraction. Mn also showed improved predictive accuracy, with R^2 values of 0.97 in PLSR and 0.94 in SVR, indicating a significant enhancement in prediction performance for low-concentration elements.

Table 3. Comparison of model performance after MLP feature extraction.

Model	Element	R_P^2	$RMSE_P$	MRE_P
PLSR	Fe	0.98	0.0072	0.0063
	Cr	0.99	0.0028	0.0027
	Ni	0.99	0.0008	0.0086
	Cu	0.99	0.0082	0.0008
	Mn	0.97	0.0045	0.0009
SVR	Fe	0.99	0.0066	0.0045
	Cr	0.99	0.0038	0.0016
	Ni	0.99	0.0013	0.0135
	Cu	0.93	0.0007	0.0120
	Mn	0.94	0.0007	0.0018

In summary, the application of MLP feature extraction enhanced the predictive performance of the models, leading to higher R^2 values and lower prediction errors, particularly for trace elements such as Cu and Mn. Feature extraction demonstrated its significant value in improving the overall accuracy and reliability of both the PLSR and SVR models.

4. Conclusions

This paper conducted a systematic study of key alloy elements such as Cr, Mn, Ni, and Cu in steel samples based on LIBS technology. From the qualitative spectra and a comparison with the NIST database, dense characteristic lines of Fe were identified in the 230 nm–290 nm wavelength range. Characteristic lines of key alloying elements were also resolved, including Cr (283.56 nm, 425.53 nm), Ni (221.64 nm, 357.87 nm), Mn (260.57 nm, 403.07 nm), and Cu (324.75 nm), providing a reliable spectral basis for multiple elements quantification. In the quantitative analysis, a comparison of SVR and PLSR showed that both models achieved high-accuracy prediction for major elements such as Fe and Cr, with $R^2 > 0.92$, whereas clear differences appeared for low-content elements Ni, Cu, and Mn. After optimization of Lv, PLSR yielded R^2 values of 0.92, 0.93, and 0.89 for Ni, Cu, and Mn, corresponding to relative improvements over SVR of approximately 8.24%, 89.80%, and 147.22%. $RMSE_P$ and MRE_P were also markedly lower under PLSR: for Ni by about 25.19% and 60.21%, for Cu by about 71.43% and 67.59%, and for Mn by about 58.06% and 13.04%. To further improve prediction accuracy and reduce dimensionality, an MLP-based feature extraction stage was placed before the PLSR and SVR models. The MLP output layer was set to 128 neurons, compressing the original 2048-dimensional spectral features to 128 dimensions, thereby reducing redundancy and

improving computational efficiency. This step markedly enhances model performance, especially for low-concentration elements. After introducing MLP feature extraction, the R^2 of Ni, Cu, and Mn increases to 0.99, 0.99, and 0.97 for PLSR and to 0.99, 0.93, and 0.94 for SVR, with RMSE and MRE markedly reduced.

Between the two algorithms, PLSR features a simpler formulation with markedly lower computational cost and faster inference, making it well-suited for real-time processing. When combined with the rapid spectral acquisition capabilities of LIBS, it offers a practical and deployable solution for online, real-time detection. Moreover, using MLP-extracted features as inputs to PLSR reduces the impact of spectral noise and redundancy, improving robustness and further enhancing prediction stability and accuracy, with significant improvements observed for elements such as Cu and Mn. Overall, the proposed "LIBS with MLP-based feature extraction and PLSR" framework delivers both high speed and high precision. It supports quality traceability and dynamic process adjustment in steel analysis and can be directly deployed in in-line monitoring and intelligent quality-control systems, demonstrating strong engineering applicability.

Author Contributions: Conceptualization, W.C.; Methodology, W.C.; Investigation, W.C.; Writing—review & editing, Y.D.; Visualization, Y.D.; Funding acquisition, Y.D. All authors have read and agreed to the published version of the manuscript.

Funding: This research was funded by Natural Science Foundation of Fujian Province (2023J05303).

Data Availability Statement: The data presented in this study are available on request from the corresponding author.

Conflicts of Interest: The authors declare no conflict of interest.

References

1. Cui, P.C.; Xing, G.S.; Nong, Z.S.; Chen, L.; Lai, Z.H.; Liu, Y.; Zhu, J.C. Recent Advances on Composition-Microstructure-Properties Relationships of Precipitation Hardening Stainless Steel. *Materials* **2022**, *15*, 8443. [CrossRef]
2. Ma, Q.; Liu, Z.Y.; Zhang, T.S.; Zhao, S.Y.; Gao, X.; Sun, T.; Dai, Y.J. Multielement simultaneous quantitative analysis of trace elements in stainless steel via full spectrum laser-induced breakdown spectroscopy. *Talanta* **2024**, *272*, 125745. [CrossRef]
3. Wang, R.M.; Luo, S.Z.; Jiang, L.Z. Cr Release from Stainless Steels. *J. Iron Steel Res. Int.* **2014**, *21*, 131–134. [CrossRef]
4. Tenaglia, N.E.; Speer, J.G.; Duran, E.H.; de Moor, E. Effects of Mn and Nb Alloying on Austenite Decomposition in High-Strength Low-Alloy (HSLA) Steels for Long Structural Applications. *Metall. Mater. Trans. A-Phys. Metall. Mater. Sci.* **2025**, *56*, 2820–2833. [CrossRef]
5. Wang, D.; Zhong, Q.D.; Yang, J.; Zhang, S.J. Effects of Cr and Ni on the microstructure and corrosion resistance of high-strength low alloy steel. *J. Mater. Res. Technol.-JMRT* **2023**, *23*, 36–52. [CrossRef]
6. Shi, X.B.; Yan, W.; Xu, D.K.; Yan, M.C.; Yang, C.G.; Shan, Y.Y.; Yang, K. Microbial corrosion resistance of a novel Cu-bearing pipeline steel. *J. Mater. Sci. Technol.* **2018**, *34*, 2480–2491. [CrossRef]
7. Singla, Y.K.; Maughan, M.R.; Arora, N.; Dwivedi, D.K. Enhancing the wear resistance of iron-based alloys: A comprehensive review of alloying element effects. *J. Manuf. Process.* **2024**, *120*, 135–160. [CrossRef]
8. Ding, Y.; Tan, Q.; Xu, J.A.; Hu, A.; Zhao, M.L.; Li, X.C.; Shu, Y.; Liu, X.X. Spectral calibration for atmospheric particles analysis under non-precise focusing conditions using LIBS combined with transfer learning. *Spectrochim. Acta Part B-At. Spectrosc.* **2025**, *228*, 107171. [CrossRef]
9. Hu, A.; Xu, J.N.; Tan, Q.; Li, X.C.; Zhao, M.L.; Shu, Y.; Liu, X.X.; Ding, Y. Spectral screening-assisted LIBS for quantitative analysis of heavy metal elements in liquid aerosols. *J. Anal. At. Spectrom.* **2025**, *40*, 2187–2196. [CrossRef]
10. Cui, M.C.; Shi, G.Y.; Deng, L.X.; Guo, H.R.; Xiong, S.L.; Tan, L.; Yao, C.F.; Zhang, D.H.; Deguchi, Y. Microstructure classification of steel samples with different heat-treatment processes based on laser-induced breakdown spectroscopy (LIBS). *J. Anal. At. Spectrom.* **2024**, *39*, 1361–1374. [CrossRef]
11. Gu, Y.H.; Chen, Z.W.; Chen, H.; Nian, F.D. Quantitative Analysis of Steel Alloy Elements Based on LIBS and Deep Learning of Multi-Perspective Features. *Electronics* **2023**, *12*, 2566. [CrossRef]
12. Chen, G.H.; Zheng, P.C.; Wang, J.M.; Li, B.; Liu, X.F.; Yang, Z.; Sun, Z.C.; Tian, H.W.; Dong, D.M.; Guo, L.B. Spectral stability improvement in laser-induced breakdown spectroscopy based on an image auxiliary data preprocessing method. *J. Anal. At. Spectrom.* **2024**, *39*, 10. [CrossRef]

13. Chen, T.; Zhang, T.; Li, H. Applications of laser-induced breakdown spectroscopy (LIBS) combined with machine learning in geochemical and environmental resources exploration. *TrAC Trends Anal. Chem.* **2020**, *133*, 116113. [CrossRef]
14. Zhang, T.; Tang, H.; Li, H. Chemometrics in laser-induced breakdown spectroscopy. *J. Chemom.* **2018**, *32*, e2983. [CrossRef]
15. Yang, L.; Zhang, Y.H.; Liu, J.M.; Zhang, Z.; Xu, M.J.; Ji, F.; Chen, J.J.; Zhang, T.D.; Lu, R.S. Spectral preprocessing to improve accuracy of quantitative detection of elemental Cr in austenitic stainless steel by laser-induced breakdown spectroscopy. *Rev. Sci. Instrum.* **2022**, *93*, 033002. [CrossRef]
16. Traparic, I.; Ivkovic, M. Determination of austenitic steel alloys composition using laser-induced breakdown spectroscopy (LIBS) and machine learning algorithms. *Eur. Phys. J. D* **2023**, *77*, 7. [CrossRef]
17. Yang, J.H.; Li, X.M.; Lu, H.L.; Xu, J.W.; Li, H.X. An LIBS quantitative analysis method for alloy steel at high temperature based on transfer learning. *J. Anal. At. Spectrom.* **2018**, *33*, 1184–1195. [CrossRef]
18. Taparli, U.A.; Kannengiesser, T.; Cieslik, K.; Mory, D.; Griesche, A. In situ chemical composition analysis of a tungsten-inert-gas austenitic stainless steel weld measured by laser-induced breakdown spectroscopy. *Spectrochim. Acta Part B-At. Spectrosc.* **2020**, *167*, 9. [CrossRef]
19. Brunnbauer, L.; Gajarska, Z.; Lohninger, H.; Limbeck, A. A critical review of recent trends in sample classification using Laser-Induced Breakdown Spectroscopy (LIBS). *TrAC Trends Anal. Chem.* **2023**, *159*, 116859. [CrossRef]
20. Li, L.-N.; Liu, X.-F.; Yang, F.; Xu, W.-M.; Wang, J.-Y.; Shu, R. A review of artificial neural network based chemometrics applied in laser-induced breakdown spectroscopy analysis. *Spectrochim. Acta Part B At. Spectrosc.* **2021**, *180*, 106183. [CrossRef]
21. Wei, L.; Ding, Y.; Chen, J.; Yang, L.Y.; Wei, J.Y.; Shi, Y.A.; Ma, Z.G.; Wang, Z.Y.; Chen, W.J.; Zhao, X.Q. Quantitative analysis of fertilizer using laser-induced breakdown spectroscopy combined with random forest algorithm. *Front. Chem.* **2023**, *11*, 1123003. [CrossRef]
22. Dyar, M.D.; Ytsma, C.R. Effect of data set size on geochemical quantification accuracy with laser-induced breakdown spectroscopy. *Spectrochim. Acta Part B-At. Spectrosc.* **2021**, *177*, 106073. [CrossRef]
23. Wudil, Y.S.; Shalabi, A.F.; Al-Osta, M.A.; Gondal, M.A.; Al-Nahari, E. Effective corrosion detection in reinforced concrete via laser-induced breakdown spectroscopy and machine learning. *Mater. Today Commun.* **2024**, *41*, 111005. [CrossRef]
24. Cortes, C.; Vapnik, V.J.M.l. Support-vector networks. *Mach. Learn.* **1995**, *20*, 273–297. [CrossRef]
25. Huang, J.W.; Dong, M.R.; Lu, S.Z.; Li, W.B.; Lu, J.D.; Liu, C.Y.; Yoo, J.H. Estimation of the mechanical properties of steel via LIBS combined with canonical correlation analysis (CCA) and support vector regression (SVR). *J. Anal. At. Spectrom.* **2018**, *33*, 720–729. [CrossRef]
26. Jia, J.W.; Liu, Z.F.; Pan, C.Y.; Xue, H.Q. Detection of Al, Mg, Ca, and Zn in copper slag by LIBS combined with calibration curve and PLSR methods. *Plasma Sci. Technol.* **2024**, *26*, 025507. [CrossRef]
27. Kashiwakura, S.; Wagatsuma, K. Selection of Atomic Emission Lines on the Mutual Identification of Austenitic Stainless Steels with a Combination of Laser-induced Breakdown Spectroscopy (LIBS) and Partial-least-square Regression (PLSR). *ISIJ Int.* **2020**, *60*, 1245–1253. [CrossRef]
28. Cole, K.D.; DeRose, P.; He, H.-J.; Stein, E.V.; Lang, B.; Schiel, J.; Urbas, A.; Solis, E.; Choquette, S.J.B.i. NIST Spectroscopic Measurement Standards. *Biopharm Int.* **2018**, *31*, 22–34.
29. Li, X.C.; Pang, M.Y.; He, Y.H.; Wang, Y.H.; Xu, J.N.; Tan, Q.; Li, J.Y.; Yu, W.Y.; Liu, X.X.; Ding, Y.; et al. Milk powder adulteration identification and quantification based on shared encoder features using Raman spectroscopy. *Spectrochim. Acta Part A-Mol. Biomol. Spectrosc.* **2026**, *348*, 10. [CrossRef] [PubMed]